# Neoclassical conductivity and bootstrap current formulas for general axisymmetric equilibria and arbitrary collisionality regime

O. Sauter[a] and C. Angioni
*Centre de Recherches en Physique des Plasmas, Association Euratom-Confédération Suisse, Ecole Polytechnique Fédérale de Lausanne, PPB, 1015 Lausanne, Switzerland*

Y. R. Lin-Liu
*General Atomics, San Diego*

(Received 15 February 1999; accepted 31 March 1999)

Expressions for the neoclassical resistivity and the bootstrap current coefficients in terms of aspect ratio and collisionality are widely used in simulating toroidal axisymmetric equilibria and transport evolution. The formulas used are in most cases based on works done 15–20 years ago, where the results have been obtained for large aspect ratio, small or very large collisionality, or with a reduced collision operator. The best expressions to date and to our knowledge are due to Hirshman [S. P. Hirshman, Phys. Fluids **31**, 3150 (1988)] for arbitrary aspect ratio in the banana regime and Hinton–Hazeltine [F. L. Hinton and R. D. Hazeltine, Rev. Mod. Phys. **48**, 239 (1976)] for large aspect ratio and arbitrary collisionality regime. A code solving the Fokker–Planck equation with the full collision operator and including the variation along the magnetic field line, coupled with the adjoint function formalism, has been used to calculate these coefficients in arbitrary equilibrium and collisionality regimes. The coefficients have been obtained for a wide variety of plasma and equilibrium parameters and a comprehensive set of formulas, which have been fitted to the code results within 5%, is proposed for evaluating the neoclassical conductivity and the bootstrap current coefficients. This extends previous works and also highlights inaccuracies in the previous formulas in this wide plasma parameter space. © *1999 American Institute of Physics.* [S1070-664X(99)03907-5]

## I. INTRODUCTION

The transport parallel to the magnetic field lines is believed to be well described by neoclassical theory. The neoclassical resistivity and bootstrap current are widely used to analyze experimental data and to design new experiments. The recent progress on advanced scenarios and steady-state operation has emphasized the importance of the bootstrap current in equilibrium calculation and its alignment with the equilibrium current. New modes, namely the neoclassical tearing modes, destabilized by the modification of the local bootstrap current around a magnetic island, have been observed (Ref. 3 and references therein). Relatively simple formulas for the neoclassical resistivity and bootstrap current exist[1–4] which are valid for low inverse aspect ratio, $\epsilon \ll 1$, and arbitrary collisionality $\nu_{e*}$, or for arbitrary plasma equilibrium and low collisionality. In Ref. 4, Harris has derived simple formulas connecting these two limits using Refs. 1 and 2. This enabled one to study any configuration,[5] as near the center one has typically $\epsilon \ll 1$ and $\nu_{e*} \sim 1$, at mid-radius $\nu_{e*} \ll 1$ and at the plasma edge $\epsilon \leqslant 1$ and $\nu_{e*} \sim 1$, even in reactor-like plasmas. A recent improvement has been to solve a set of multispecies fluid equations using the three odd velocity moments of the Fokker–Planck equation,[6] following the work of Hirshman, using interpolation formulas for viscosity moments from low and large collisionality regimes. In this way one obtains the resistivity and bootstrap current for arbitrary shape and collisionality,[7] in addition to multispecies effects. However, as a set of equations have to be solved in a specific code, NCLASS, it is not of convenient use for rapid experimental diagnostics or tokamak design over a wide range of parameters. Also it does not use the full collision operator which can lead to errors up to 20% as mentioned in Ref. 6 and first shown in Ref. 8. This is why we have extended the work published in Refs. 9, 10 in order to have a complete, accurate and analytical set of formulas for the neoclassical resistivity and all the bootstrap current coefficients.

The model is briefly presented in Sec. II and the results are given in Sec. III.

## II. PHYSICS MODEL

The code CQLP solves the Fokker–Planck equation using the linearized operator on a magnetic flux surface, including the advection parallel to the magnetic field.[9] It does not make any assumption on the ratio of the collision frequency to the bounce frequency. Moreover the code uses the magnetic geometry as calculated by a toroidal equilibrium code and, therefore, uses the exact axisymmetric magnetic configuration of the flux surface. One has to solve the linearized Fokker–Planck equation for arbitrary $\epsilon$ and $\nu_{e*}$ [Ref. 2, Eq. (5.21)–(24)]

[a]Author to whom correspondence should be addressed. Electronic mail address: Olivier.Sauter@epfl.ch

 

$$v_\parallel \hat{\mathbf{b}}\cdot\nabla f_{e1} - C_e^l(f_{e1}) = -(v_D\cdot\nabla\psi)_e \frac{\partial f_{e0}}{\partial\psi} - \frac{q_e E_\parallel}{m_e}\frac{\partial f_{e0}}{\partial v_\parallel}, \tag{1}$$

$$v_\parallel \hat{\mathbf{b}}\cdot\nabla f_{i1} - C_{ii}^l(f_{i1}) = -(v_D\cdot\nabla\psi)_i \frac{\partial f_{i0}}{\partial\psi}, \tag{2}$$

with

$C_e^l = C_{ee}^l + C_{ei}^l$:

Linearized collision operator (Rosenbluth potentials),

$$(v_D\cdot\nabla\psi)_\sigma = I(\psi) v_\parallel \hat{\mathbf{b}}\cdot\nabla\left(\frac{v_\parallel}{\Omega_\sigma}\right),$$

$$\frac{\partial f_{\sigma 0}}{\partial\psi} = f_{\sigma 0}\left[\frac{\partial \ln n_{\sigma 0}}{\partial\psi} + \frac{q_\sigma}{T_\sigma}\frac{\partial\langle\Phi\rangle}{\partial\psi} + \left(\frac{v^2}{v_{T_\sigma}^2} - \frac{3}{2}\right)\frac{\partial \ln T_{\sigma 0}}{\partial\psi}\right],$$

and where $v_{T\sigma}^2 = 2T^2/m_\sigma$ and $\Omega_\sigma = q_\sigma B_0/m_\sigma$ are the thermal velocity and the cyclotron frequency of species $\sigma$, $I(\psi) = RB_\phi$, $\hat{\mathbf{b}} = \mathbf{B}/B$, and $\langle\Phi\rangle$ is the flux surface averaged electrostatic potential. Note that we do not take into account the modifications due to potato orbits and, therefore, our results should be slightly modified near the magnetic axis according to Ref. 11. Following the work in Ref. 12 adapted to this problem in Ref. 8 and also described in Ref. 9, one can solve the following adjoint equations [using the same notations as in Ref. 9 and Eq. (4.45) of Ref. 2]:

$$-v_\parallel \hat{\mathbf{b}}\cdot\nabla\chi_e - C_{e0}^l(\chi_e) = q_e v_\parallel B f_{e0}, \tag{3}$$

$$-v_\parallel \hat{\mathbf{b}}\cdot\nabla\chi_i - C_{ii}^l(\chi_i) = q_i v_\parallel B f_{i0}. \tag{4}$$

Then the flux surface averaged parallel current is given by

$$\langle j_\parallel B\rangle = \sigma_{\rm neo}\langle E_\parallel B\rangle - I(\psi) p_e(\mathcal{L}_{31}A_1 + \mathcal{L}_{32}A_2 + \mathcal{L}_{34}A_4), \tag{5}$$

with

$$A_1 = \frac{1}{p_e}\frac{\partial p_e}{\partial\psi} + \frac{1}{p_e}\frac{\partial p_i}{\partial\psi},$$

$$A_2 = \frac{1}{T_e}\frac{\partial T_e}{\partial\psi}, \quad A_2^i = \frac{1}{T_i}\frac{\partial T_i}{\partial\psi}, \tag{6}$$

$$A_4 = \alpha\frac{1-R_{pe}}{R_{pe}}A_2^i,$$

where we have used $T_i/ZT_e = (1/R_{pe} - 1)$ with $R_{pe} = p_e/p$, and the coefficients are obtained from the adjoint functions $\chi_e$ and $\chi_i$

$$\sigma_{\rm neo} = \frac{q_e}{T_e}\left\langle \frac{1}{B}\int v_\parallel \chi_e \mathbf{dv}\right\rangle, \tag{7}$$

$$\mathcal{L}_{31} = -1 - \frac{1}{Ip_e}\left\langle \int \frac{\chi_e}{f_{e0}} C_{e0}^l(\gamma_1 f_{e0})\mathbf{dv}\right\rangle$$

$$= -1 + \frac{1}{Ip_e}\left\langle \int \chi_e Z_i \nu_{e0}\gamma_1 \frac{v_{Te}^3}{v^3}\mathbf{dv}\right\rangle, \tag{8}$$

$$\mathcal{L}_{32} = -\frac{1}{Ip_e}\left\langle \int \frac{\chi_e}{f_{e0}} C_{e0}^l(\gamma_{2e} f_{e0})\mathbf{dv}\right\rangle$$

$$= \frac{1}{Ip_e}\left\langle \int \chi_e \nu_{e0}\gamma_1\left[-h\left(\frac{v}{v_{Te}}\right) + Z_i\frac{v_{Te}^3}{v^3}\left(\frac{v^2}{v_{Te}^2} - \frac{5}{2}\right)\right]\mathbf{dv}\right\rangle$$

$$\equiv \mathcal{L}_{32\_ee} + \mathcal{L}_{32\_ei}, \tag{9}$$

$$\mathcal{L}_{34} = -1 - \frac{1}{Ip_e}\left\langle \int \frac{\chi_e}{f_{e0}} C_{e0}^l(\gamma_4 f_{e0})\mathbf{dv}\right\rangle$$

$$= -1 + \frac{1}{Ip_e}\left\langle \frac{B^2}{\langle B^2\rangle}\int \chi_e Z_i \nu_{e0}\gamma_1\frac{v_{Te}^3}{v^3}\mathbf{dv}\right\rangle, \tag{10}$$

$$\alpha = -\frac{1}{Ip_i}\left\langle \int \frac{\chi_i}{f_{i0}} C_{ii}^l(\gamma_{2i} f_{i0})\mathbf{dv}\right\rangle$$

$$= -\frac{q_e}{\nu_i T_e}\left\langle \int \chi_i \nu_{i0} h\left(\frac{v}{v_{Ti}}\right)\frac{v_\parallel}{\Omega_i}\mathbf{dv}\right\rangle, \tag{11}$$

with

$$\gamma_1 = \frac{I(\psi)v_\parallel}{\Omega_e}, \quad \gamma_{2e} = \gamma_1\left(\frac{v^2}{v_{Te}^2} - \frac{5}{2}\right),$$

$$\gamma_4 = \gamma_1\frac{B^2}{\langle B^2\rangle}, \quad \gamma_{2i} = \frac{I(\psi)v_\parallel}{\Omega_i}\left(\frac{v^2}{v_{Ti}^2} - \frac{5}{2}\right),$$

where $h(x) = x^{-3}[10\,\mathrm{erf}(x) - 10x\,\mathrm{erf}'(x) - 4x^2\,\mathrm{erf}(x)]$, $\nu_{e0} = 3\sqrt{\pi}/(4Z_i\tau_e)$, $\nu_{i0} = 3\sqrt{\pi/2}/(2\tau_i)$, and $\mathcal{L}_{32\_ee} \sim \langle\int \chi_e C_{ee}^l\rangle$, $\mathcal{L}_{32\_ei} \sim \langle\int \chi_e C_{ei}^l\rangle$. The code solves Eq. (3) for the electron adjoint function, using Maxwellian background ions of charge $Z$ for the $e$-$i$ collision contribution, and Eq. (4) for the ions. Then the coefficients, Eqs. (7)–(11) are computed using the solutions $\chi_e$ and $\chi_i$. Changing the flux surface considered or the plasma equilibrium, one can vary the aspect ratio or the trapped fraction $f_t$, where $f_t$ is defined as

$$f_t = 1 - f_c = 1 - \frac{3}{4}\langle B^2\rangle\int_0^{1/B_{\max}}\frac{\lambda\, d\lambda}{\langle\sqrt{1-\lambda B}\rangle}. \tag{12}$$

We have used this exact definition, but an approximate and fairly accurate value can be obtained from simpler terms as described in Ref. 13. Also varying the temperature and density, one can change the collisionality regime from the banana regime to $\nu_{e*} \gg 1$, where $\nu_{e*} = 0.012 n_{e20} Z_{\rm eff} qR/\epsilon^{3/2} T_{ekeV}^2$. Finally, we have varied the ion charge $Z$, to obtain the dependence on $Z_{\rm eff}$. The results obtained with CQLP for the coefficients Eqs. (7)–(11) in this three-dimensional parameter space are given in the next Section, as well as the formulas used to fit the results in terms of $f_t$, $\nu_{e*}$, and $Z_{\rm eff}$. The code CQL3D[14] has also been modified to solve the bounce-averaged version of Eqs. (3)–(11) and compute in the collisionless limit the coefficients. As this reduces to solving a two-dimensional (2D) problem in the velocity space, the results are more accurate and much faster to obtain and it gives a benchmark for CQLP in the limit $\nu_{e*} \ll 0.01$.

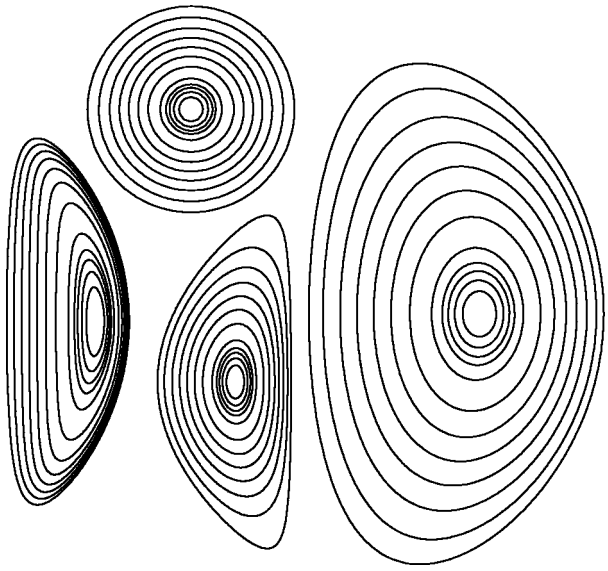

FIG. 1. Examples of different equilibria used in this paper.

## III. RESULTS

We have solved Eqs. (3) and (4) over a wide variety of equilibria, trapped fraction $f_t$ (i.e., on different flux surfaces), and collisionalities in order to determine accurately the fitted formulas for the neoclassical resistivity $\sigma_{\rm neo}$, and the bootstrap current coefficient $\mathcal{L}_{31}$, $\mathcal{L}_{32}$, $\mathcal{L}_{34}$ and $\alpha$, relative to the pressure, the electron, and the ion temperature gradients, Eqs. (7)–(11). Some of the different equilibria considered are shown in Fig. 1. These range from circular low $\beta$ and large aspect ratio to high $\beta$ small aspect ratio and highly elongated plasma, with low and high triangularities. Therefore, same values of $\epsilon$ as well as $f_t$ have been studied in different toroidal equilibria.

First, following the work in Ref. 1, we show in Fig. 2

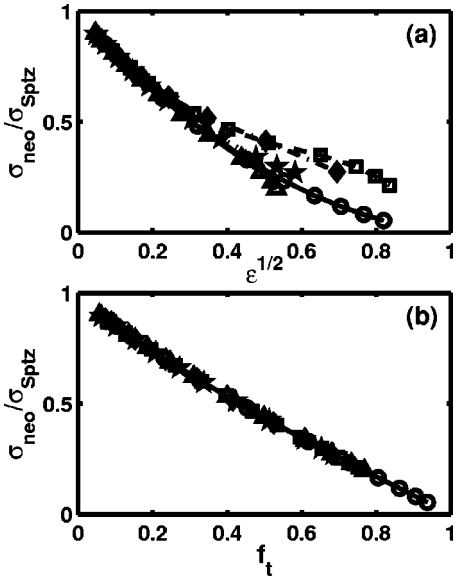


FIG. 2. Neoclassical conductivity as obtained by CQL3D, normalized to the Spitzer conductivity, vs (a) square root of the inverse aspect ratio, and (b) trapped fraction $f_t$. The different symbols refer to different equilibria in all the Figures.

that the trapped fraction $f_t$ is a good parameter to encapsulate the geometrical effects on conductivity in the collisionless limit. In Fig. 2(a), we show the neoclassical conductivity obtained by CQL3D, using the bounce-averaged version of Eqs. (3) and (7), versus the square root of the inverse aspect ratio $\epsilon$. As one can see clearly, $\sigma_{\rm neo}$ depends not only on $\epsilon$ but also on other equilibrium parameters. On the other hand, when plotted versus $f_t$, then all the points are well-aligned and $\sigma_{\rm neo}$ depends only on $f_t$. The same is obtained for the bootstrap current coefficients, within 1%, which shows that $f_t$ does represent the effective trapped fraction for noncircular and finite $\epsilon$ equilibria.

Different options have been used to include finite collisionality effects in the formulas,[2,4,10,15] but mostly the coefficients in the formulas have been modified. As $f_t$ is a very good parameter in the collisionless limit, it seems better to change only $f_t$ as a function of $\nu_{e*}$ if possible. In this way one can first find the polynomial dependence of $\sigma_{\rm neo}$, $\mathcal{L}_{31}$, $\mathcal{L}_{32}$, and $\alpha$ on $f_t$ in the collisionless limit using CQL3D, which is faster and more accurate. And then determine the effective trapped fraction $f_t(\nu_{e*})$ for finite collisionality, while keeping the coefficient of the polynomials independent of $\nu_{e*}$. This procedure is also easier to find an analytic formula valid for arbitrary $f_t$ and $\nu_{e*}$, as one does essentially two one-dimensional (1D) fits, instead of one 2D fit. Finally it is interesting as one naturally obtains the effect of collisionality on the fraction of trapped particles. This procedure was shown to be possible for $\sigma_{\rm neo}$ and $\mathcal{L}_{31}$ in Ref. 10. Since then we have made more detailed calculations and also modified the code to solve Eq. (4) for the ions.

In the banana regime, the results of CQL3D for the coefficient $\mathcal{L}_{32}$ confirm the inaccuracy of the formulas of Refs. 1 and 6, which is more significant at small values of $Z$, as shown in Fig. 3. This is due to the complexity of this term, which consists of two contributions of opposite signs, $\mathcal{L}_{32\_ee}$ and $\mathcal{L}_{32\_ei}$, Eq. (9), each of which having different contributions from the small and large $v$ regions as shown in Fig. 4. In particular the term $\mathcal{L}_{32\_ee}$ has its main contribution from the high energy tail in the region $v/v_{\rm th}\sim 2$, and therefore, it explains the discrepancies, in agreement with the results of Ref. 16. The term $\alpha$ is similar to the term $\mathcal{L}_{32\_ee}$ and we also find about 20% differences between the exact solution of Eqs. (4) and (9) and the formula in Ref. 1 in the banana regime. Moreover it can be inferred from Fig. 4 that both terms will have a different collisionality dependence as their main contribution come from different $v$ region. Increasing collisionality modifies first the small $v$ region and therefore modifies first $\mathcal{L}_{32\_ei}$. This is shown in Fig. 5 where both terms, $\mathcal{L}_{32\_ee}$ and $\mathcal{L}_{32\_ei}$, are plotted vs $\nu_{e*}$. Of course, the limit at high collisionality of $\mathcal{L}_{32}$ is zero and, therefore, $\mathcal{L}_{32\_ee}=-\mathcal{L}_{32\_ei}$ for $\nu_{e*}\gg 10$. We also show our fit and the fit derived in Ref. 4 from the formulas in Refs. 1 and 2. We see that the peculiar dependence of $\mathcal{L}_{32}$ on $\nu_{e*}$, as it even changes sign, is easier determined by the simple $\nu_{e*}$ dependence of $\mathcal{L}_{32\_ee}$ and $\mathcal{L}_{32\_ei}$. This is why we have separated the coefficient $\mathcal{L}_{32}$ into two terms having different collisionality dependence, that is different effective trapped

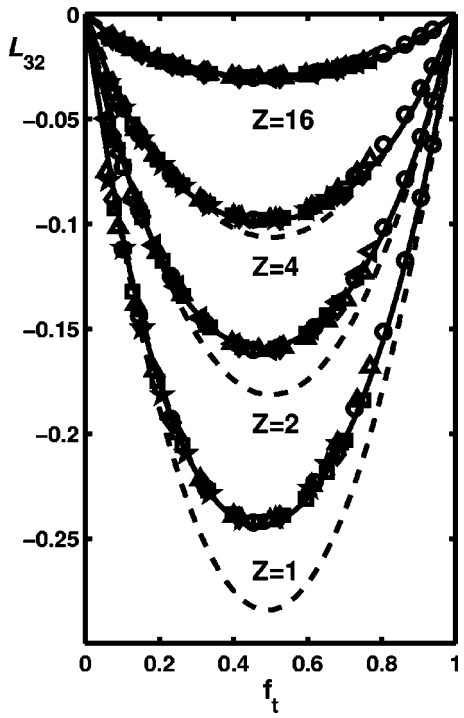


FIG. 3. Bootstrap current coefficient $\mathcal{L}_{32}$ vs $f_t$ for different charge number $Z$ in the collisionless limit (CQL3D). The solid lines are obtained from Eqs. (15) with $f_{\text{teff}}^{32\_ee}=f_{\text{teff}}^{32\_ei}=f_t$. The dashed lines are obtained from Hirshman's formula (Ref. 1).

fractions. The analytical fits to the results of CQL3D and CQLP, valid for arbitrary $f_t$, $\nu_{e*}$, and $Z$ are given as follows:

$$\frac{\sigma_{\text{neo}}(f_{\text{teff}}^{33})}{\sigma_{\text{Sptz}}}=F_{33}(X=f_{\text{teff}}^{33})\equiv 1-\left(1+\frac{0.36}{Z}\right)X+\frac{0.59}{Z}X^2-\frac{0.23}{Z}X^3, \tag{13a}$$

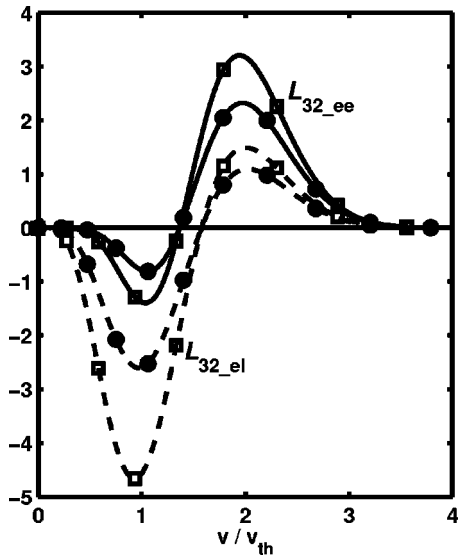


FIG. 4. Velocity dependence, normalized to $v_{\text{th}}=\sqrt{2T_e/m_e}$, of the integrands of $\mathcal{L}_{32\_ee}$, solid lines, and $\mathcal{L}_{32\_ei}$, dashed lines, for low (solid circles) and high (open squares) collisionality cases.

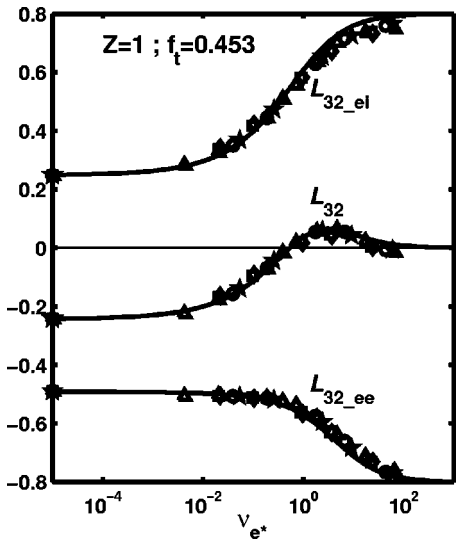


FIG. 5. Bootstrap current coefficient $\mathcal{L}_{32}=\mathcal{L}_{32\_ee}+\mathcal{L}_{32\_ei}$ vs collisionality $\nu_{e*}$. The solid lines are obtained from Eqs. (15). For Eqs. (15b) and (15c), the terms $\mp 1.2/(1+0.5Z)$ have been added, respectively.

$$f_{\text{teff}}^{33}(\nu_{e*})=\frac{f_t}{1+(0.55-0.1f_t)\sqrt{\nu_{e*}}+0.45(1-f_t)\nu_{e*}/Z^{3/2}}, \tag{13b}$$

$$\mathcal{L}_{31}=F_{31}(X=f_{\text{teff}}^{31})\equiv\left(1+\frac{1.4}{Z+1}\right)X-\frac{1.9}{Z+1}X^2+\frac{0.3}{Z+1}X^3+\frac{0.2}{Z+1}X^4, \tag{14a}$$

$$f_{\text{teff}}^{31}(\nu_{e*})=\frac{f_t}{1+(1-0.1f_t)\sqrt{\nu_{e*}}+0.5(1-f_t)\nu_{e*}/Z}, \tag{14b}$$

$$\mathcal{L}_{32}=F_{32\_ee}(X=f_{\text{teff}}^{32\_ee})+F_{32\_ei}(Y=f_{\text{teff}}^{32\_ei}), \tag{15a}$$

$$F_{32\_ee}(X)=\frac{0.05+0.62Z}{Z(1+0.44Z)}(X-X^4)+\frac{1}{1+0.22Z}[X^2-X^4-1.2(X^3-X^4)]+\frac{1.2}{1+0.5Z}X^4, \tag{15b}$$

$$F_{32\_ei}(Y)=-\frac{0.56+1.93Z}{Z(1+0.44Z)}(Y-Y^4)+\frac{4.95}{1+2.48Z}[Y^2-Y^4-0.55(Y^3-Y^4)]-\frac{1.2}{1+0.5Z}Y^4, \tag{15c}$$

$$f_{\text{teff}}^{32\_ee}(\nu_{e*})=\frac{f_t}{1+0.26(1-f_t)\sqrt{\nu_{e*}}+0.18(1-0.37f_t)\nu_{e*}/\sqrt{Z}}, \tag{15d}$$

$$f_{\text{teff}}^{32\_ei}(\nu_{e*}) = \frac{f_t}{1+(1+0.6f_t)\sqrt{\nu_{e*}}+0.85(1-0.37f_t)\nu_{e*}(1+Z)}, \tag{15e}$$

$$\mathcal{L}_{34} = F_{31}(X = f_{\text{teff}}^{34}), \tag{16a}$$

$$f_{\text{teff}}^{34}(\nu_{e*}) = \frac{f_t}{1+(1-0.1f_t)\sqrt{\nu_{e*}}+0.5(1-0.5f_t)\nu_{e*}/Z}, \tag{16b}$$

$$\alpha_0 = -\frac{1.17(1-f_t)}{1-0.22f_t-0.19f_t^2}, \tag{17a}$$

$$\alpha(\nu_{i*}) = \left[\frac{\alpha_0+0.25(1-f_t^2)\sqrt{\nu_{i*}}}{1+0.5\sqrt{\nu_{i*}}} - 0.315\nu_{i*}^2 f_t^6\right]\frac{1}{1+0.15\nu_{i*}^2 f_t^6}, \tag{17b}$$

where

$$\sigma_{\text{Sptz}} = 1.9012\cdot 10^4 \frac{T_e[\text{eV}]^{3/2}}{ZN(Z)\ln\Lambda_e}[\text{m}^{-1}\Omega^{-1}], \tag{18a}$$

$$N(Z) = 0.58 + \frac{0.74}{0.76+Z},$$

$$\nu_{e*} = 6.921\cdot 10^{-18}\frac{qRn_eZ\ln\Lambda_e}{T_e^2\epsilon^{3/2}}, \tag{18b}$$

$$\nu_{i*} = 4.90\cdot 10^{-18}\frac{qRn_iZ^4\ln\Lambda_{ii}}{T_i^2\epsilon^{3/2}}, \tag{18c}$$

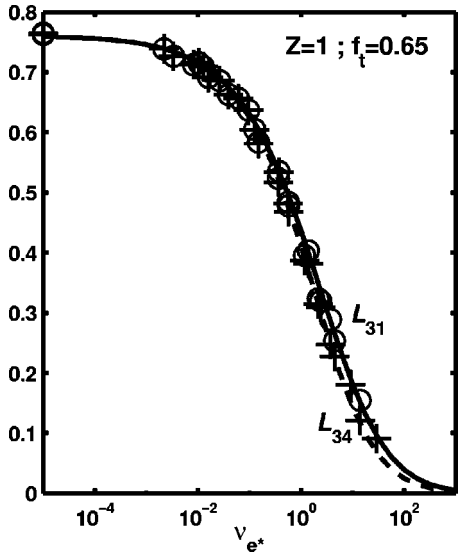


FIG. 6. The coefficients $\mathcal{L}_{31}$, open circles, and $\mathcal{L}_{34}$, crosses, vs collisionality $\nu_{e*}$, as obtained with CQLP. The solid line corresponds to Eq. (14) and the dashed line to Eq. (16).

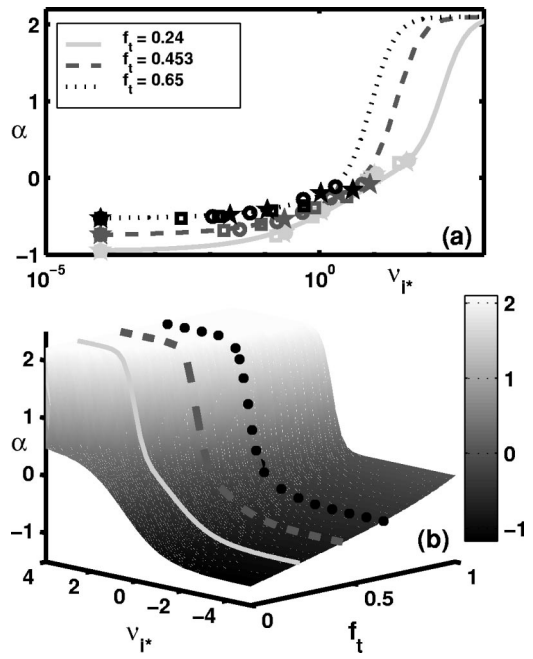


FIG. 7. (a) Coefficient $\alpha$ for three different values of $f_t$ vs $\nu_{i*}$. The solid lines correspond to Eq. (17) and they are reproduced on the 3D plot. (b) 3D view of the coefficient $\alpha$ in terms of $f_t$ and $\nu_{i*}$ for $Z=1$. Note that the sharp rise depends strongly on both $f_t$ and $\nu_{i*}$.

$$\ln\Lambda_e = 31.3 - \ln\left(\frac{\sqrt{n_e}}{T_e}\right), \tag{18d}$$

$$\ln\Lambda_{ii} = 30 - \ln\left(\frac{Z^3\sqrt{n_i}}{T_i^{3/2}}\right), \tag{18e}$$

with $q$ being the safety factor, densities in $m^{-3}$ and temperatures in eV. We have tested different definitions of $\nu_{e*}$ and $\nu_{i*}$, using some averaged poloidal magnetic field instead of $rB/qR$ and/or some function of $f_t$ instead of $\epsilon^{3/2}$, for example. However, the simple definition used here with the combination of $Rq$ and $\epsilon^{-3/2}$, Eqs. (18b) and (18c), gives the best overlap of the results of the different equilibria at same values of $f_t$ and $\nu_{e*}$, as shown in Figs. 5–7(a). We see also from Eqs. (14b) and (16b) that $\mathcal{L}_{34}$ is indeed almost equal to $\mathcal{L}_{31}$, except at very large $\nu_{e*}$, as seen in Fig. 6 and in agreement with Ref. 2. This is why we only had to change slightly the collisionality dependence of $f_{\text{teff}}^{31}$, as it can be shown, using the bounce-averaged equations, that $\mathcal{L}_{34}=\mathcal{L}_{31}$ in the collisionless limit.

Finally we have not used the same structure for the coefficient $\alpha$. First it should be emphasized that the actual coefficient for the ion temperature gradient is $\mathcal{L}_{34}\alpha$. Second, as seen in Fig. 7(a), the coefficient has a very sharp $\nu_{i*}$ dependence, which is very sensitive also to $f_t$ as shown in Fig. 7(b). It is, therefore, not possible to decouple the $f_t$ and $\nu_{i*}$ dependences as is done for the other coefficients. This is why we have modified the formula proposed by Harris[4] such as to reproduce the correct results in the banana regime, Eq. (17a), as well as in the plateau region, and such as to have a function of $f_t$ rather than $\epsilon$ in order to be valid for any axisymmetric geometry.

## IV. CONCLUSION

We have extended the work of Refs. 1 and 2 in solving Eqs. (3) and (4) using the exact Fokker–Planck operator and without any approximation on the plasma geometry or collisionality. In this way we have been able to accurately determine the neoclassical resistivity and the coefficients for the bootstrap current which allows one to calculate

$$\langle j_{\|}B\rangle = \sigma_{\rm neo}\langle E_{\|}B\rangle - I(\psi)p_e\left[\mathcal{L}_{31}\frac{p}{p_e}\frac{\partial \ln p}{\partial \psi} + \mathcal{L}_{32}\frac{\partial \ln Te}{\partial \psi} + \mathcal{L}_{34}\alpha\frac{\partial \ln Ti}{\partial \psi}\right],$$

where the coefficients are given in Eqs. (13)–(17) as functions of $f_t$, Eq. (12), $\nu_{e*}$ and $\nu_{i*}$, Eq. (18), and $Z$. Note that the parallel current can also be written as follows, assuming $\partial \ln n_e/\partial\psi = \partial \ln n_i/\partial\psi$:

$$\langle j_{\|}B\rangle = \sigma_{\rm neo}\langle E_{\|}B\rangle - I(\psi)p(\psi)\left[\mathcal{L}_{31}\frac{\partial \ln n_e}{\partial \psi} + R_{pe}(\mathcal{L}_{31} + \mathcal{L}_{32})\frac{\partial \ln T_e}{\partial \psi} + (1-R_{pe}) \times\left(1+\frac{\mathcal{L}_{34}}{\mathcal{L}_{31}}\alpha\right)\mathcal{L}_{31}\frac{\partial \ln T_i}{\partial \psi}\right].$$

As $\mathcal{L}_{31}\approx\mathcal{L}_{34}\approx -0.5$, $\mathcal{L}_{32}\approx 0.2$, $\alpha\approx -0.5$, and $R_{pe}\approx 0.5$, one sees that the coefficient of the bootstrap current driven by the density gradient is about $-0.5$, while it is around $-0.15$ for $T_e$ and $-0.1$ for $T_i$. Therefore, density gradients are more efficient in driving bootstrap current, which can be significant for the neoclassical tearing modes as mentioned in Ref. 3.

For multispecies cases we could use our code to solve the coupled equations, but it is out of the scope of this paper. Also a comparison of our formulas with the results of the NCLASS code should enable one to determine the correct form of the value of $Z$, instead of $Z_{\rm eff}$, to be used in our expressions, in the same way as mentioned in Ref. 2. This should be performed while taking into account the inaccuracy of the like-particle collision operator in NCLASS. Such a comparison would also determine the effect of the potato orbits near the magnetic axis and indicate how $f_t$ should be adapted there.

## ACKNOWLEDGMENTS

We are grateful to R. W. Harvey, F. L. Hinton, and J. Vaclavik for useful discussions. This work was supported in part by the Swiss National Science Foundation.

[1] S. P. Hirshman, Phys. Fluids **31**, 3150 (1988).
[2] F. L. Hinton and R. D. Hazeltine, Rev. Mod. Phys. **48**, 239 (1976).
[3] O. Sauter, R. J. La Haye, Z. Chang *et al.*, Phys. Plasmas **4**, 1654 (1997).
[4] G. R. Harris, private communication [see Eq. (10) of Refs. 5 and 22 therein].
[5] C. E. Kessel, Nucl. Fusion **34**, 1221 (1994).
[6] W. A. Houlberg, K. C. Shaing, S. P. Hirshman, and M. C. Zarnstorff, Phys. Plasmas **4**, 3230 (1997).
[7] K. C. Shaing, C. T. Hsu, M. Yokoyama, and M. Wakatani, Phys. Plasmas **2**, 349 (1995); K. C. Shaing, M. Yokoyama, M. Wakatani, and C. T. Hsu, *ibid.* **3**, 965 (1996).
[8] Y. R. Lin-Liu, private communication.
[9] O. Sauter, R. W. Harvey, and F. L. Hinton, Contrib. Plasma Phys. **34**, 169 (1994).
[10] O. Sauter, Y. R. Lin-Liu, F. L. Hinton, and J. Vaclavik, in *Proceedings of the Theory of Fusion Plasmas workshop*, Varenna 1994 (Editrice Compositori E. Sindoni, Bologna, 1994), p. 337.
[11] K. C. Shaing, C. T. Hsu, and R. D. Hazeltine, Phys. Plasmas **1**, 3365 (1994).
[12] C. F. F. Karney, N. J. Fisch, and A. H. Reiman, in *Proceedings of the 8th Top. Conference on RF Power in Plasma*, Irvine, 1989 (American Institute of Physics, Woodbury, NY, 1989), p. 430.
[13] Y. R. Lin-Liu and R. L. Miller, Phys. Plasmas **2**, 1666 (1995).
[14] R. W. Harvey and M. G. McCoy, in *Proceedings of IAEA Technical Committee Meeting on Advances in Simulation and Modeling of Thermonuclear Plasmas*, Montreal, 1992 (International Atomic Energy Agency, Vienna, 1993), pp. 489–526.
[15] S. P. Hirshman, R. J. Hawryluk, and B. Birge, Nucl. Fusion **17**, 611 (1977).
[16] S. P. Hirshman and D. J. Sigmar, Phys. Fluids **19**, 1532 (1976).